



# Theoretical Investigation on H<sub>2</sub>O<sub>2</sub>-Ng (He, Ne, Ar, Kr, Xe, and Rn) Complexes Suitable for Stereodynamics: Interactions and Thermal Chiral Rate Consequences

Yuri Alves de Oliveira Só<sup>1</sup>, Pedro Henrique de Oliveira Neto<sup>1</sup>,  
Luiz Guilherme Machado de Macedo<sup>2</sup> and Ricardo Gargano<sup>1\*</sup>

<sup>1</sup> Institute of Physics, University of Brasília, Brasília, Brazil, <sup>2</sup> Institute of Biological Sciences, Faculty of Biotechnology, Federal University of Pará, Belém, Brazil

## OPEN ACCESS

### Edited by:

Antonio Aguilar,  
University of Barcelona, Spain

### Reviewed by:

Vincenzo Aquilanti,  
University of Perugia, Italy  
Luca Evangelisti,  
University of Bologna, Italy

### \*Correspondence:

Ricardo Gargano  
gargano@unb.br

### Specialty section:

This article was submitted to  
Physical Chemistry and Chemical  
Physics,  
a section of the journal  
Frontiers in Chemistry

Received: 08 November 2018

Accepted: 24 December 2018

Published: 18 January 2019

### Citation:

Só YAdO, Neto PHdO,  
de Macedo LGM and Gargano R  
(2019) Theoretical Investigation on  
H<sub>2</sub>O<sub>2</sub>-Ng (He, Ne, Ar, Kr, Xe, and Rn)  
Complexes Suitable for  
Stereodynamics: Interactions and  
Thermal Chiral Rate Consequences.  
Front. Chem. 6:671.  
doi: 10.3389/fchem.2018.00671

Although molecular collisions of noble gases (Ng) can be theoretically used to distinguish between the enantiomers of hydrogen peroxide - H<sub>2</sub>O<sub>2</sub> (HP), little is known about the effects of HP-Ng interactions on the chiral rate. In this work, the chiral rate as a function of temperature (CRT) between enantiomeric conformations of HP and Ng (Ng=He, Ne, Ar, Kr, Xe, and Rn) are presented at MP2(full)/aug-cc-pVTZ level of theory through a fully basis set superposition error (BSSE) corrected potential energy surface. The results show that: (a) the CRT is highly affected even at a small decrease in the height of trans-barrier; (b) its smallest values occur with Ne for all temperatures between 100 and 4,000 K; (c) that the decrease of CRT shows an inverse correlation with respect to the average valence electron energy of the Ng and (d) Ne and He may be the noble gases more suitable for study the oriented collision dynamics of HP. In addition to binding energies, the electron density  $\rho$  and its Laplacian  $\nabla^2\rho$  topological analyses were also performed within the atoms in molecules (AIM) theory in order to determine the nature of the HP-Ng interactions. The results of this work provide a more complete foundation on experiments to study HP's chirality using Ng in crossed molecular beams without a light source.

**Keywords:** hydrogen peroxide, noble gases, stereodynamics, chirality, thermal chiral rate, enantiomers, TST method, AIM theory

## 1. INTRODUCTION

Hydrogen peroxide - H<sub>2</sub>O<sub>2</sub> (HP) is a molecule of interest in a large and diverse number of fields in addition to its industrial uses. For example, it has emerged as a major metabolite in redox signaling and regulation (Antunes and Brito, 2017; Sies, 2017), and its presence was observed in Martian atmosphere (Encrenaz et al., 2004) and also on the surface of Jupiter's moon Europa (Carlson et al., 1999). The HP is interesting since it is simplest molecule that exhibits internal (torsional) rotation and chirality. Furthermore, this molecule can form dimers (Dobado and Molina, 1993; González et al., 1997), clusters (Yu and Yang, 2011), complexes with water (Mo et al., 1994; González et al., 1997) and with biologically important molecules such as adenine (Dobado and Molina, 1999), DNA (Piatnytskyi et al., 2016), glycine (Shi and Zhou, 2004) or nitrosamines (Roohi et al., 2010). These features indicate that HP should be a better proton donor for hydrogen bonding than

water. Thus, the understanding of how the relative orientation of the O-H can lead to a weakly complex or a chemical reaction has also been paid considerable attention due to its implication in atmospheric chemistry and oxidation reactions (Lundell et al., 1998, 2001; Daza et al., 2000; Goebel et al., 2000, 2001a,b, 2002; Molina et al., 2002; Pehkonen et al., 2004; Mucha and Mielke, 2009; Grzechnik et al., 2013). Moreover, HP's properties have been investigated, such as its isolated chirality (Roncaratti and Aquilanti, 2010), stereomutation (Fehrensens et al., 2007; Bitencourt et al., 2008), size-dimensional wave packets (Wang et al., 2012), spectroscopy (Hunt et al., 1965; Małyszczak and Koput, 2013; Al-Refaie et al., 2015) and rotation barriers (Song et al., 2005).

On the other hand, the hydrogen peroxide seems to be a prototypical model to be used into experiments to observe chirality in crossed molecular beam without a light source (Palazzetti et al., 2013), a frontier in research of stereodynamics which is still at early stages (Su et al., 2013; Lombardi and Palazzetti, 2018). In these kind of experiments, the molecular orientation control on the intense continuous beam is mandatory to the phenomena of chiral selectivity to be demonstrated (Aquilanti et al., 2005). For this reason, the interaction between HP and atoms, molecules and ions is so relevant to stereodynamics studies (Barreto et al., 2007, 2010; Lombardi et al., 2011; Roncaratti et al., 2014; Leal et al., 2016).

In the present paper we investigated the dynamics of the chiral molecule HP interacting by van der Waals forces with noble gases Ng (Ng=He, Ne, Ar, Kr, Xe and Rn) in order to obtain the chiral rate as a function of temperature (CRT) for these complexes, as well as its consequences for the chiral kinetic interconversion when tunneling effect is included. The aim of this work was to understand how the kinetic interconversion of the two HP's isomers is affected along collisional events through a basis set superposition error (Boys and Bernardi, 1970) (BSSE) corrected potential energy surface (PES). In addition, the electron density  $\rho(r)$  and its Laplacian  $\nabla^2\rho(r)$  topological analyses were also performed within the atoms in molecules (AIM) theory in order to determine the nature of the intermolecular interactions.

## 2. METHODOLOGY

### 2.1. Computational Details

All calculations were performed using the Gaussian09 package (Frisch et al., 2009). The structures were optimized without constraints at MP2(full) method in conjunction with aug-cc-pVTZ-PP for Xe and Rn (Peterson et al., 2003) and aug-cc-pVTZ for the remaining atoms (Dunning, 1989; Woon and Dunning Jr, 1993; Wilson et al., 1999). Vibrational frequencies at the same level of theory were also performed in order to ensure that each minimum has only positive frequencies and that each transition state has only a single imaginary frequency, as well as to obtain the zero point vibrational energy (ZPE). The counterpoise method of Boys and Bernardi (1970) was used to correct the BSSE for binding energy.

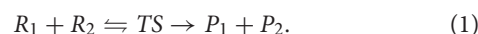
AIM analysis (Matta and Boyd, 2007) and graphic representations were performed with the AIMALL program (Keith, 2017) using the MP2(full) density (wavefunction) as

input as described in the AIM theory (Dobado et al., 1998; Cortés-Guzmán and Bader, 2005).

### 2.2. Overview of the Transition State Theory

The transition state theory (TST)(Truhlar et al., 1996) was developed primarily by Henry Eyring (Eyring, 1935) and Michael Polanyi (Polanyi and Wigner, 1928) between 1928 and 1935. The TST is an improvement over the so-called theory of collisions (Lewis, 1967), and it is widely used to calculate the rate constants of chemical reactions.

The start point of TST is the existence of a transition state (TS) between the reagents and products. Located at the top of the potential energy barrier and it assumes a quasi-equilibrium between reactants and activated transition state complexes. For a bimolecular reaction given by



The TS is characterized by a single imaginary frequency along the reaction coordinate of the molecular system which is represented here by  $\bar{\nu}_1$ . In its turn, the reaction coordinate can be represented by angular changes in bond distances during the chemical reaction (Henkelman et al., 2002).

The equation that determines the reaction rate is known as the Eyring equation, given by

$$k_{\text{rate}}(T) = \kappa(T) \frac{k_B T}{h} \frac{\bar{q}_{m,TS}^\circ}{q_{m,R_1}^\circ q_{m,R_2}^\circ} N_A e^{-E_b^0/RT}, \quad (2)$$

where  $0 < \kappa(T) \leq 1$  is the so-called transmission coefficient,  $k_B$  is the Boltzmann constant,  $h$  is the Planck constant,  $q_m^\circ$  is the standard molar partition function,  $N_A$  is the Avogadro constant,  $R$  is the gas constant and  $E_b^0$  is the barrier energy with zero-point energy correction. In addition, the TS,  $R_1$  and  $R_2$  subscripts stand for the transition state and reagents, respectively. Thus, the rate constant is determined by the parameters that characterize both reagents and the TS.

The general partition function is formed by the product of translational  $q^{\text{trans}}$ , rotational  $q^{\text{rot}}$ , vibrational  $q^{\text{vib}}$  and electronic  $q^{\text{ele}}$  partition functions. The translational partition function for a free particle with mass  $m$  moving along the length dimension  $l_x$  can be evaluated by considering that the separation of energy levels is small and that a large number of states are accessible at room temperatures. Therefore, the energy levels should be continuous and the sum contribution of the translational partition function becomes an integral. Which the solution for the three-dimensional case is (Atkins et al., 2013)

$$q^{\text{trans}} = \frac{(2\pi mk_B T)^{3/2}}{h^3} l_x l_y l_z. \quad (3)$$

Although the system can be excited at normal modes, the energy levels are discrete for the rotational mode. The three degrees of freedom of spatial rotation and the three moments of inertia  $I_A$ ,  $I_B$  and  $I_C$  must be taken into account for a non-linear molecule (Atkins et al., 2013), thus

$$q^{\text{rot}} = \frac{(\pi)^{1/2}}{\sigma} \left( \frac{8\pi^2 I_A I_B I_C k_B T}{h^2} \right)^{3/2}, \quad (4)$$

where  $\sigma$  is the so-called number of symmetry. The vibrational mode has reasonably spaced energy which must be taken into account since they are partially occupied. As a consequence, the vibrational partition function is strictly calculated as a sum over the occupied states. In the case of  $n$  vibrational degrees of freedom, the vibrational partition function is given by the product of  $n$  partition functions,

$$q^{\text{vib.}} = \prod_i^n \frac{1}{1 - e^{-h\nu_i/k_B T}}, \quad (5)$$

where  $\nu_i$  is each of the fundamental vibrational frequencies. In most cases, only the lowest energy state is occupied and the electronic energies should not contribute considerably to the total partition function (Atkins et al., 2013). A good approximation is to disregard the contributions of the nuclear and electronic spins and to vanish the fundamental energy level for the electronic partition function. Under these considerations the electronic partition function should be equal to unity (Atkins et al., 2013)

$$q^{\text{ele.}} = 1. \quad (6)$$

On the other hand, the coefficient  $\kappa(T)$  represents the tunneling effect of the reaction coordinate of the chemical system and it is usually important for light atoms or molecules at low temperatures. Thus, tunneling estimates were made using both Wigner (Polanyi and Wigner, 1928) and Eckart (Eckart, 1930) methods.

The Wigner tunneling correction proposes a parabolic potential,

$$V_{\text{Wigner}}(s) = E_b - \frac{1}{2}m(2\pi\bar{\nu}_1)^2s^2, \quad (7)$$

where  $E_b$  corresponds the energy potential barrier of MEP,  $\bar{\nu}_1$  is the imaginary frequency of transition state and  $s$  is the coordinate

reaction. This implies in a transmission coefficient given by Bell (1959)

$$\kappa_{\text{Wigner}}(T) = 1 - \frac{1}{24} \left( \frac{h\bar{\nu}_1}{k_B T} \right)^2, \quad (8)$$

For very low temperatures, the Wigner tunneling effect is not very effective, and for this reason, it was also employed Eckart tunneling correction (Truhlar et al., 1985).

The Eckart tunneling correction uses a potential of the type

$$V(x) = \frac{Ae^{\alpha x}}{1 + e^{\alpha x}} + \frac{Be^{\alpha x}}{(1 + e^{\alpha x})^2}, \quad (9)$$

where  $\alpha$  is a parameter described by

$$\alpha^2 = -\frac{\mu(\bar{\nu}_1)^2 B}{2E_b^0(E_b^0 - A)} \quad (10)$$

and  $\mu$  is the reduced mass of the system. These parameters determine the barrier width. Here it is important to note that the  $A$  and  $B$  can be positive, negative or zero. The  $A$  parameter corresponds to the energy difference  $V(x \rightarrow -\infty)$  and  $V(x \rightarrow +\infty)$ , and  $B$  is a parameter that measures the height of the barrier given by

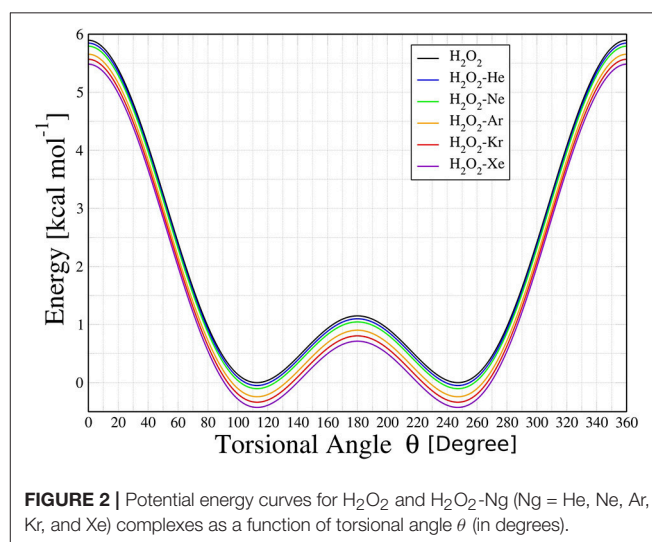
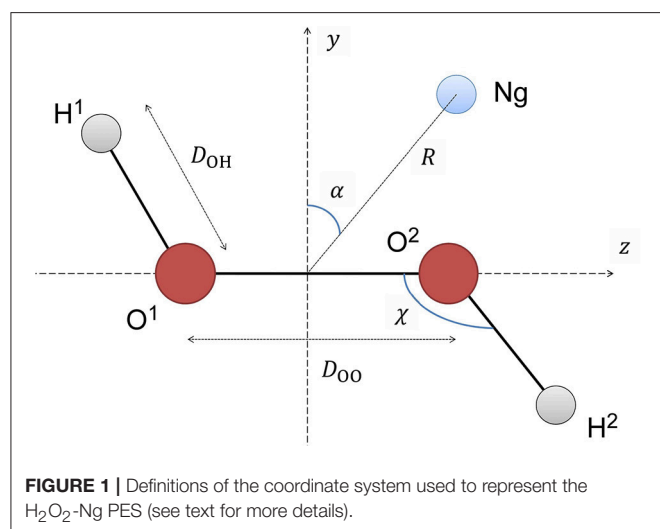
$$B = 2E_b^0 - A + 2\sqrt{E_b^0(E_b^0 - A)}. \quad (11)$$

So the most usual form for the Eckart's potential in the study of reaction rates is (Truhlar et al., 1985)

$$V_{\text{Eckart}}(s) = \frac{Ae^{\alpha(s-s_0)}}{1 + e^{\alpha(s-s_0)}} + \frac{Be^{\alpha(s-s_0)}}{[1 + e^{\alpha(s-s_0)}]^2}, \quad (12)$$

where  $s$  is the coordinate of the reaction and  $s_0$  is the reaction coordinate corresponding to the maximum of the barrier, which is given by

$$s_0 = -\frac{1}{\alpha} \ln \left( \frac{A+B}{A-B} \right). \quad (13)$$



Finally, the transmission probability (Bell, 1980), obtained through the solution of the Schrödinger equation with Eckart's potential, is expressed by the following equation

$$P_{\text{Eckart}}(E) = 1 - \frac{\cosh[2\pi(k - \beta)] + \cosh(2\pi\delta)}{\cosh[2\pi(k + \beta)] + \cosh(2\pi\delta)}, \quad (14)$$

where  $k$ ,  $\beta$  and  $\delta$  depend on  $\bar{v}_1$ ,  $A$ ,  $B$  and energy ( $E$ ).

The quantum tunneling correction  $\kappa(T)$  can thus be calculated from the ratio between the quantum rate  $k_{\text{quan.}}(T)$  and the classical rate  $k_{\text{class.}}(T)$  in which the particles cross the barrier. Thus, the Eckart tunneling correction with transmission

coefficient is given by

$$\kappa(T) = \frac{k_{\text{quan.}}(T)}{k_{\text{class.}}(T)} = \frac{e^{E_b/k_B T}}{k_B T} \int_0^\infty dE P_{\text{Eckart}}(E) e^{-E/k_B T}, \quad (15)$$

where integration is performed over all possible energies.

### 3. RESULTS AND DISCUSSION

#### 3.0.1. Geometric Parameters, Interactions and AIM Analysis

The details about the generation of the potential energy surface are described in another work of our group (Roncaratti et al., 2014), so it will be commented briefly here. First, all HP geometry

**TABLE 1** | Geometrical parameters (in Å and degree) obtained at MP2(full)/aug-cc-pVTZ level for isolated HP and HP-Ng (Ng=He, Ne, Ar, and Kr) complexes and MP2(full)/aug-cc-pVTZ-PP level for HP-Ng (Ng=Xe and Rn) complexes.

|                                 | HP        | HP-He     | HP-Ne     | HP-Ar     | HP-Kr     | HP-Xe     | HP-Rn     |
|---------------------------------|-----------|-----------|-----------|-----------|-----------|-----------|-----------|
| <b>cis-barrier</b>              |           |           |           |           |           |           |           |
| O-O                             | 1.4570    | 1.4568    | 1.4568    | 1.4566    | 1.4566    | 1.4566    | 1.4567    |
| O-H                             | 0.9641    | 0.9641    | 0.9641    | 0.9644    | 0.9647    | 0.9652    | 0.9654    |
| Ng-HO                           | -         | 2.5712    | 2.6819    | 2.7932    | 2.8856    | 3.0340    | 3.0930    |
| ∠ O-O-H                         | 104.2159  | 104.1917  | 104.1643  | 104.0088  | 103.9379  | 103.8664  | 103.8273  |
| ∠ Ng-H-O                        | -         | 143.7666  | 144.7561  | 145.8957  | 146.5895  | 147.6918  | 148.1087  |
| ∠ H-O-O-H                       | 0.0000    | 0.0000    | 0.0000    | 0.0000    | 0.0000    | 0.000     | 0.0000    |
| <b>θ<sub>-</sub></b>            |           |           |           |           |           |           |           |
| O-O                             | 1.4478    | 1.4478    | 1.4477    | 1.4478    | 1.4479    | 1.4479    | 1.4479    |
| O-H                             | 0.9641    | 0.9641    | 0.9641    | 0.9645    | 0.9648    | 0.9653    | 0.9656    |
| Ng-HO                           | -         | 2.5299    | 2.6410    | 2.7361    | 2.8338    | 2.9901    | 3.0506    |
| ∠ O-O-H                         | 99.7698   | 99.7484   | 99.7609   | 99.6817   | 99.6684   | 99.6708   | 99.6725   |
| ∠ Ng-H-O                        | -         | 148.5851  | 149.1316  | 151.3108  | 152.5323  | 153.3889  | 153.4619  |
| ∠ H-O-O-H                       | 112.5091  | 112.6401  | 112.6131  | 112.6964  | 112.6133  | 112.4499  | 112.3769  |
| <b>trans-barrier</b>            |           |           |           |           |           |           |           |
| O-O                             | 1.4578    | 1.4584    | 1.4585    | 1.4586    | 1.4587    | 1.4589    | 1.4590    |
| O-H                             | 0.9632    | 0.9633    | 0.9633    | 0.9637    | 0.9639    | 0.9644    | 0.9646    |
| Ng-HO                           | -         | 2.5545    | 2.6410    | 2.7619    | 2.8581    | 3.0161    | 3.0775    |
| ∠ O-O-H                         | 98.1418   | 98.1251   | 98.1150   | 98.0630   | 98.0376   | 98.0253   | 98.0198   |
| ∠ Ng-H-O                        | -         | 140.9618  | 142.7619  | 145.7730  | 147.4343  | 148.6294  | 148.8774  |
| ∠ H-O-O-H                       | 180.0000  | 180.0000  | 179.9996  | 179.9933  | 180.0000  | 180.0000  | 180.0044  |
| <b>θ<sub>+</sub></b>            |           |           |           |           |           |           |           |
| O-O                             | 1.4478    | 1.4478    | 1.4477    | 1.4478    | 1.4479    | 1.4479    | 1.4479    |
| O-H                             | 0.9641    | 0.9641    | 0.9641    | 0.9645    | 0.9648    | 0.9653    | 0.9656    |
| Ng-H-O                          | -         | 2.5299    | 2.6410    | 2.7361    | 2.8338    | 2.9901    | 3.0515    |
| ∠ O-O-H                         | 99.7698   | 99.7484   | 99.7619   | 99.6817   | 99.6684   | 99.6708   | 99.6704   |
| ∠ Ng-H-O                        | -         | 148.5851  | 149.1521  | 151.3108  | 152.5323  | 153.3889  | 153.4538  |
| ∠ H-O-O-H                       | -112.5091 | -112.6401 | -112.6107 | -112.6964 | -112.6133 | -112.4499 | -112.3768 |
| <b>Other work<sup>(a)</sup></b> |           |           |           |           |           |           |           |
| <b>θ<sub>-</sub></b>            |           |           |           |           |           |           |           |
| O-O                             | -         | 1.441     | 1.441     | 1.441     | -         | -         | -         |
| O-H                             | -         | 0.964     | 0.964     | 0.964     | -         | -         | -         |
| Ng-H-O                          | -         | 2.576     | 2.596     | 2.828     | -         | -         | -         |
| ∠ O-O-H                         | -         | 100.1     | 100.1     | 100.1     | -         | -         | -         |
| ∠ Ng-H-O                        | -         | 151.3     | 155.5     | 150.9     | -         | -         | -         |
| ∠ H-O-O-H                       | -         | 111.8     | 111.8     | 111.9     | -         | -         | -         |

<sup>(a)</sup> Values obtained by Molina et al. (2002) at MP2/6-311+G(3df,2p) level with BSSE corrections.

parameters were kept frozen at their equilibrium values of  $D_{OO} = 1.45\text{Å}$ ,  $D_{OH} = 0.966\text{Å}$  and the angle  $\text{HOO} = 100.8^\circ$ . The Ng's position is expressed in terms of the polar coordinates as represented in **Figure 1**, where  $R$  is the distance of Ng relative to the middle of O-O bond and  $\alpha$  is the polar angle with respect to an axis perpendicular to the O-O bond ( $z$  axis). The two planes defined by O-O-H atoms are then rotated around the O-O axis, with steps of  $1^\circ$ . In addition,  $\alpha$  was equal to  $0^\circ$ ,  $45^\circ$ ,  $90^\circ$  and  $R$  distance was varied from 2 to  $5\text{Å}$  with steps  $0.1\text{Å}$ .

Topological studies performed on this adjusted potential energy surface (PES) showed that the HP and HP-Ng complexes have two overall minimum configurations, termed *cis* (labeled as  $\theta_-$ ) and *trans* (labeled as  $\theta_+$ ), separated by two potential barriers,

**TABLE 2** | Binding energies (in kcal/mol) of HP–Ng complexes obtained at MP2(full)/aug–cc–pVTZ level for HP–Ng (Ng=He, Ne, Ar, and Kr) and MP2(full)/aug–cc–pVTZ–PP level for HP–Ng (Ng=Xe and Rn)<sup>a</sup>.

|                       | BSSE | $D_e$ | $D_e^{\text{BSSE}}$ | $D_0$ | $D_0^{\text{BSSE}}$ | Other work <sup>(b)</sup> |
|-----------------------|------|-------|---------------------|-------|---------------------|---------------------------|
| <b>HP–He</b>          |      |       |                     |       |                     |                           |
| <i>cis</i>            | 0.10 | −0.19 | −0.09               | 0.10  | 0.20                |                           |
| <i>trans</i>          | 0.10 | −0.19 | −0.09               | 0.10  | 0.20                | −0.04 <sup>(b)</sup>      |
| <i>cis</i> -barrier   | 0.12 | −0.26 | −0.14               | 0.03  | 0.15                |                           |
| <i>trans</i> -barrier | 0.07 | −0.18 | −0.11               | 0.09  | 0.18                |                           |
| <b>HP–Ne</b>          |      |       |                     |       |                     |                           |
| <i>cis</i>            | 0.30 | −0.47 | −0.17               | −0.18 | 0.12                |                           |
| <i>trans</i>          | 0.30 | −0.47 | −0.17               | −0.18 | 0.12                | −0.10 <sup>(a)(b)</sup>   |
| <i>cis</i> -barrier   | 0.36 | −0.63 | −0.27               | −0.34 | 0.02                |                           |
| <i>trans</i> -barrier | 0.29 | −0.49 | −0.20               | −0.20 | 0.09                |                           |
| <b>HP–Ar</b>          |      |       |                     |       |                     |                           |
| <i>cis</i>            | 0.62 | −1.18 | −0.56               | −0.89 | −0.27               |                           |
| <i>trans</i>          | 0.62 | −1.18 | −0.56               | −0.89 | −0.27               | −0.38 <sup>(b)</sup>      |
| <i>cis</i> -barrier   | 0.78 | −1.63 | −0.85               | −1.34 | −0.56               |                           |
| <i>trans</i> -barrier | 0.59 | −1.19 | −0.60               | −0.90 | −0.31               |                           |
| <b>HP–Kr</b>          |      |       |                     |       |                     |                           |
| <i>cis</i>            | 1.41 | −2.12 | −0.71               | −1.83 | −0.42               |                           |
| <i>trans</i>          | 1.41 | −2.12 | −0.71               | −1.83 | −0.42               |                           |
| <i>cis</i> -barrier   | 1.79 | −2.89 | −1.10               | −2.60 | −0.81               |                           |
| <i>trans</i> -barrier | 1.39 | −2.15 | −0.76               | −1.86 | −0.47               |                           |
| <b>HP–Xe</b>          |      |       |                     |       |                     |                           |
| <i>cis</i>            | 1.23 | −2.11 | −0.88               | −1.82 | −0.59               |                           |
| <i>trans</i>          | 1.23 | −2.11 | −0.88               | −1.82 | −0.59               |                           |
| <i>cis</i> -barrier   | 1.64 | −3.04 | −1.40               | −2.75 | −1.11               |                           |
| <i>trans</i> -barrier | 1.23 | −2.14 | −0.91               | −1.85 | −0.62               |                           |
| <b>HP–Rn</b>          |      |       |                     |       |                     |                           |
| <i>cis</i>            | 1.63 | −2.58 | −0.95               | −2.29 | −0.66               |                           |
| <i>trans</i>          | 1.63 | −2.58 | −0.95               | −2.29 | −0.66               |                           |
| <i>cis</i> -barrier   | 2.23 | −3.77 | −1.58               | −3.48 | −1.25               |                           |
| <i>trans</i> -barrier | 1.65 | −2.64 | −0.99               | −2.35 | −0.70               |                           |

<sup>a</sup>Where  $D_e$  is the electronic binding energy,  $D_0=D_e+ZPE$  is the electronic binding energy with the zero point energy ZPE,  $D_e^{\text{BSSE}}=D_e+\text{BSSE}$  and  $D_0^{\text{BSSE}}=D_0+\text{BSSE}$  are the electronic binding energies with BSSE correction.

<sup>(b)</sup>Values obtained by Molina et al. (2002) at MP2/6–311+G(3df,2p) level, for some complexes, with BSSE corrections.

denoted here as *cis*-barrier and *trans*-barrier. The potential energy curves (PEC) obtained from the PES are then presented in **Figure 2**.

The PECs obtained for HP-Ng complexes are similar in shape and depth. The *cis*-barriers for the HP-Ng complexes are all smaller than the respective value for the free HP. The free HP has a *cis*-barrier of 7.5594 kcal/mol whereas the values for the complexes increase monotonically from 6.9828 kcal/mol for HP-Rn up to 7.5107 kcal/mol for HP-He. In addition the *trans*-barrier values are also lower than the respective value for the free HP, which is 1.0427 kcal/mol, and their values are 1.0928 kcal/mol for HP-He, 1.0817 kcal/mol for HP-Ne, 1.0651 kcal/mol for HP-Ar, 1.0676 kcal/mol for HP-Kr, 1.0736 kcal/mol for HP-Rn and 1.0749 kcal/mol for HP-Xe complexes. For the free HP, the *cis*-barrier and *trans*-barrier experimental energies (Hunt et al., 1965) are  $7.0334 \pm 0.0715$  kcal/mol and  $1.1036 \pm 0.0114$  kcal/mol, respectively. These values are in a good agreement with our results. However, for

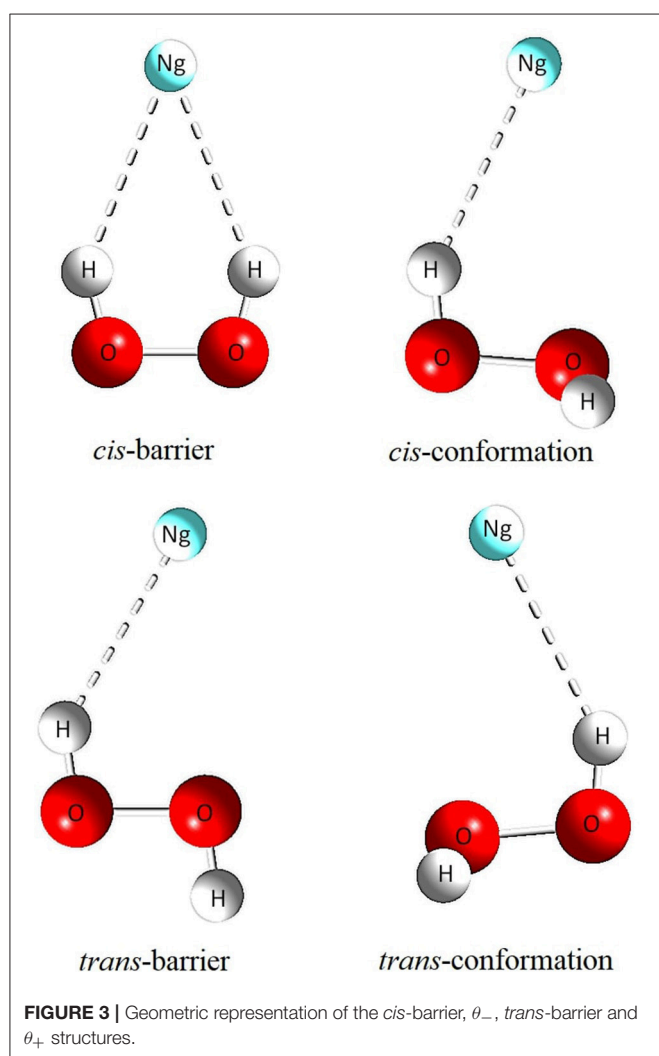
**TABLE 3** | Bond critical point (BCP) data for charge density  $\rho$  (in  $\times 10^{-3}e/a_0^3$ ), Laplacian of the charge density  $\nabla^2\rho$  (in  $\times 10^{-2}e/a_0^5$ ), electronic energy density  $H(r)$  and ellipticity  $\epsilon$  for configurations 1(*cis*), 2(*cis*-barrier), 3(*trans*) and 4(*trans*-barrier) of the HP-Ng complexes.

| Complexes | Configuration | Description   | $\rho$ | $\nabla^2\rho$ | $H(r)$ | $\epsilon$ |
|-----------|---------------|---------------|--------|----------------|--------|------------|
| He–HP     | 1             | (3,−1) He...H | 2.1    | 1.12           | 0.0007 | 0.448      |
|           |               | (3,+1) ring   | 2.0    | 1.11           | 0.0007 |            |
|           | 2             | (3,−1) He...H | 2.1    | 1.12           | 0.0008 | 0.0965     |
|           |               | (3,−1) He...H | 2.0    | 1.10           | 0.0008 | 0.2306     |
| Ne–HP     | 1             | (3,−1) Ne...H | 2.1    | 1.12           | 0.0008 | 0.0965     |
|           |               | (3,+1) ring   | 2.6    | 1.48           | 0.0007 |            |
|           | 2             | (3,−1) Ne...H | 2.9    | 1.51           | 0.0008 | 0.1397     |
|           |               | (3,−1) Ne...H | 3.0    | 1.54           | 0.0008 | 0.1397     |
| Ar–HP     | 1             | (3,−1) Ar...H | 2.9    | 1.51           | 0.0008 | 0.0738     |
|           |               | (3,+1) ring   | 4.8    | 2.02           | 0.0009 |            |
|           | 2             | (3,−1) Ar...H | 5.9    | 2.36           | 0.0012 | 0.0179     |
|           |               | (3,−1) Ar...H | 5.6    | 2.24           | 0.0012 | 0.0439     |
| Kr–HP     | 1             | (3,−1) Kr...H | 5.9    | 2.36           | 0.0012 | 0.0179     |
|           |               | (3,−1) Kr...H | 6.44   | 2.22           | 0.0009 | 0.1628     |
|           | 2             | (3,−1) Kr...H | 5.35   | 2.08           | 0.0008 |            |
|           |               | (3,−1) Kr...H | 6.63   | 2.34           | 0.0010 | 0.0124     |
| Xe–HP     | 1             | (3,−1) Xe...H | 6.35   | 2.24           | 0.0010 | 0.0285     |
|           |               | (3,−1) Xe...H | 6.63   | 2.34           | 0.0010 | 0.0285     |
|           | 2             | (3,−1) Xe...H | 7.0    | 2.02           | 0.0006 | 0.1460     |
|           |               | (3,−1) Xe...H | 5.7    | 1.99           | 0.0006 |            |
| Rn–HP     | 1             | (3,−1) Rn...H | 7.0    | 2.09           | 0.0007 | 0.0095     |
|           |               | (3,−1) Rn...H | 6.7    | 2.00           | 0.0007 | 0.0178     |
|           | 2             | (3,−1) Rn...H | 7.0    | 2.09           | 0.0007 | 0.0095     |
|           |               | (3,−1) Rn...H | 7.1    | 1.90           | 0.0005 | 0.1417     |
| Rn–HP     | 1             | (3,−1) Rn...H | 5.9    | 1.91           | 0.0005 |            |
|           |               | (3,−1) Rn...H | 7.1    | 1.96           | 0.0006 | 0.0105     |
|           | 2             | (3,−1) Rn...H | 6.8    | 1.88           | 0.0006 | 0.0126     |
|           |               | (3,−1) Rn...H | 7.1    | 1.96           | 0.0006 | 0.0103     |

the HP-Ng complexes we did not find experimental data for comparison.

The results concerning geometric parameters, interactions and their characterization are summarized in **Tables 1–3**. The geometrical parameters obtained at MP2(full)/aug-cc-pVTZ, optimized without any constraints for two minimum structures and transition states (presented as *cis* and *trans* barriers) are given in **Table 1** together with the graphical representation in **Figure 3**. **Table 2** lists the binding energies corrected and uncorrected for the BSSE. **Table 3** shows the numerical results for AIM analysis and **Figure 4** depicts the  $\nabla^2\rho(r)$  contour plots for *cis* and *trans* barrier configurations.

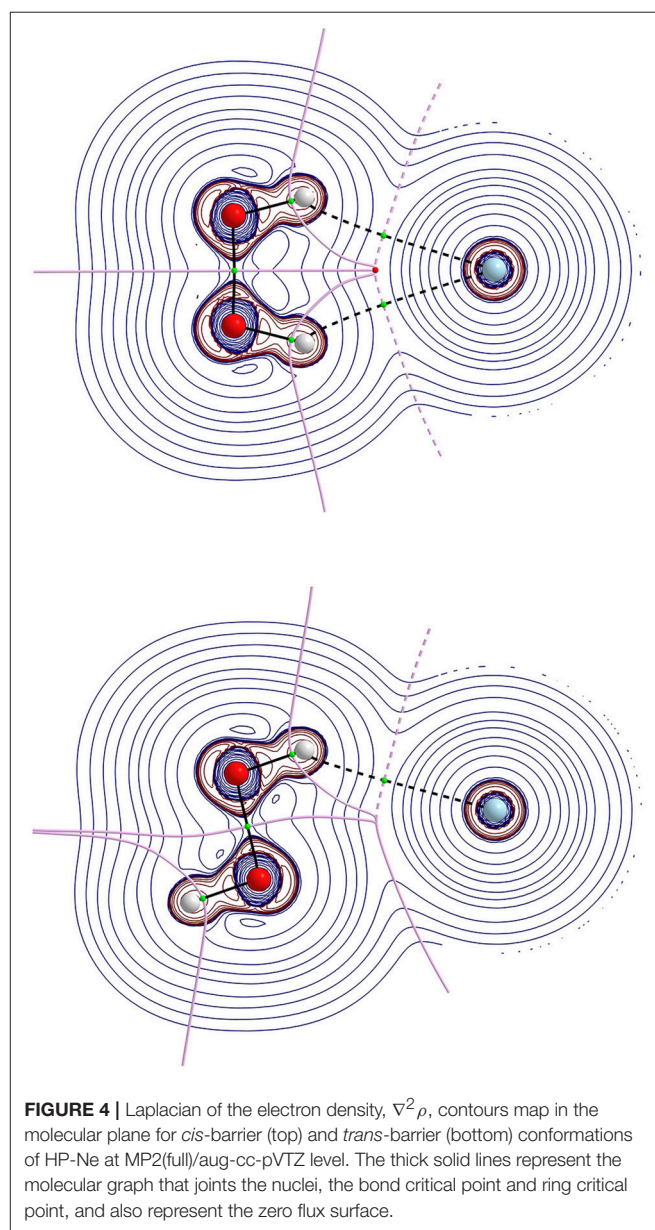
The PESs yield  $\theta_-$  and  $\theta_+$  as true minima, i.e. without any imaginary frequencies in accordance with results from literature (Maciel et al., 2006; Roncaratti et al., 2014). In addition, all transition state structures displayed a well characterized imaginary frequency around 600 cm<sup>-1</sup> for *cis* and 400 cm<sup>-1</sup> for *trans* barriers (see **Supplementary Information** for further details). **Figure 5** describes a schematic representation of vibrational modes of the isolated HP in the transition state with the actual frequencies and an imaginary



frequency, which represents the frequency along the reaction coordinate.

For the HP-Ng complexes, the geometrical parameters are almost the same when compared with isolated HP in agreement with the weak interaction of these systems. The HP-Ng distances increase from He up Rn. On average, they are close to 2.55Å(He), 2.65Å(Ne), 2.75Å(Ar), 2.85Å(Kr), 3.00Å(Xe), and 3.06Å(Rn).

Regarding the binding energies, HP-He and HP-Ne are all repulsive, being less repulsive for the *cis* barrier configuration. This can be understood as a consequence of the fact that the noble gases turn out to be the hardest elements (Furtado et al., 2015) and this hardness decreases when the Ng atomic number is increased (the hardness in this context is a resistance to changes in its electronic population Furtado et al., 2015 coupled to Ng's high electronegativity Allen and Huheey, 1980). Although the BSSE increases monotonically from He to Rn, the binding



energies also become more attractive as the atomic number increases.

For the four structures of each HP-Ng, the higher binding values are always observed for the *cis*-barrier configuration. As it will pointed latter, the decrease of the rate through the two barriers are not correlated with the binding energy, suggesting the hyperconjugation effects on HP may be important for the decrease of the interaction rate.

Regarding the AIM analysis, the existence of (3,−1) bond critical point (BCP) and its associated atomic interaction line indicates that electronic charge density is accumulated between the linked nuclei (Bader, 1991). In its turn, the values of the charge density  $\rho(r)$  in BCP are small while their corresponding  $\nabla^2\rho(r)$  are positive in accordance with a closed shell type of interaction. As a consequence, all configurations of all complexes show an interaction of a van der Waals type. Since higher ellipticity suggests conjugation and hyperconjugation effects of electron delocalization, these effects seem more pronounced in the HP-He and HP-Ne complexes. Another interesting feature is that all *cis*-barrier configurations of all complexes show a (3,+1) BCP indicating a cyclic nature.

### 3.0.2. Thermal Chiral Rate Analysis

The temperature dependence of the rate constant for *cis* to *trans* (i.e., through *trans*-barrier) and *trans* to *cis* (i.e., through *cis*-barrier) conformations for HP and HP-Ng complexes are presented in **Figure 6**. These results, in addition to conventional rate, are also exhibited with Eckart's or Wigner's tunneling corrections.

It was found that for the entire 100 K up to 4,000 K range the HP-Ne has the lowest rates for both barriers among all noble gas complexes, followed by HP-He. This result suggests that Ne and He are the noble gases more suitable for study the oriented

collision dynamics with HP. In fact, the decrease of CRT shows an inverse correlation with respect the average valence electron energy (Allen, 1989), which follows the sequence (from higher to lower values): Ne, He, Ar, Kr; with Xe and Rn having very close values.

Nevertheless, there is a trend of rate increase as are move from Ar up to Rn. It is interesting to note that although this behavior is very similar regarding the *cis*-barrier for all rates (conventional, Wigner e Eckart), it seems that the tunneling is more important to describe the *trans* barrier's rate, where there is a significant difference for Eckart's values specially in the 100–200 K range when compared to respective Wigner and conventional results.

The final thermal rate constant can be expressed in the two familiar Arrhenius forms. In this work, the first is the Arrhenius modified form given by

$$k(T) = AT^n e^{-E_a/RT}, \quad (16)$$

where  $A$  is the pre-exponential factor,  $T$  a temperature,  $n$  is a real number,  $R$  is the universal gas constant and  $E_a$  is the activation energy. The second is the d-Arrhenius form (Aquilanti et al., 2010; Silva et al., 2013; Carvalho-Silva et al., 2017) expressed by

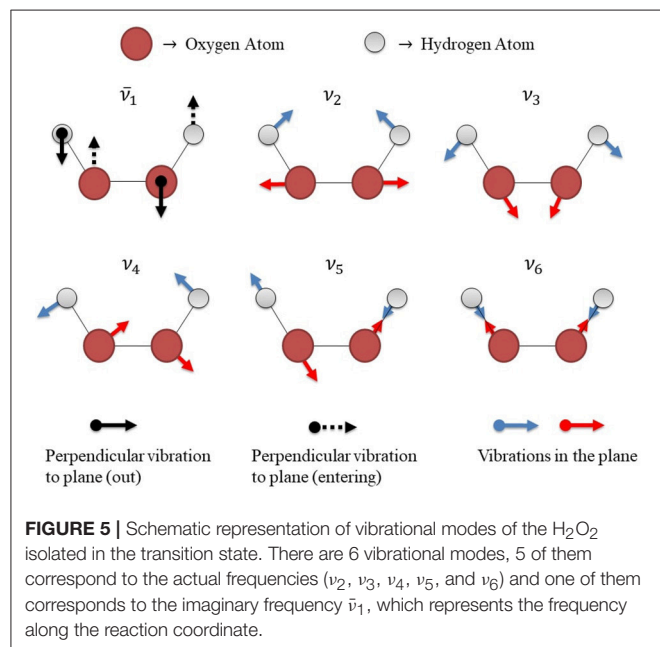
$$k(T) = A \left(1 - d \frac{E_a}{RT}\right)^{1/d} \quad (17)$$

where  $d$  is a parameter that yield the degree of deformation of the exponential function.

The curve obtained by the reaction rate constant vs. the temperature can be fitted (Ramalho et al., 2011) to obtain the parameters  $A$ ,  $n$  and  $E_a$  for the Arrhenius modified form, as presented in **Table 4**, and the parameters  $A$ ,  $d$ , and  $E_a$  for d-Arrhenius form, as presented in **Table 5**. This feature confirms the trend of lower  $k(T)$  observed for HP-Ng complexes for both barriers when compared to isolated HP.

It can be also observed in **Figure 6** that the *trans* to *cis* conformation rate of HP is lower (in the range 100–200 K) than the corresponding ones for HP-Ar, HP-Kr, HP-Xe, and HP-Rn. In the case of the chiral transition from *cis* to *trans*, the rates of all HP-Ng complexes are lower than that of the isolated HP. These results showed that the transition rate from *cis* to *trans* is greater than the corresponding *trans* to *cis* for both the isolated HP molecule and for all HP-Ng complexes. This suggests that the most important barrier that separates the chiral configurations of the isolated HP and the HP-Ng complexes is the *trans*-barrier, since it is the smallest. The energy of the HP's *trans*-barrier is relatively small (1.0427 kcal/mol) compared to its *cis*-barrier (7.5595 kcal/mol) as already seen in **Figure 2**.

An interesting result is presented in the **Table 6**. Although the increase in the *trans*-barrier of the HP-Ng complexes relative to HP is considerably small (see **Figure 7**), the change in the transition rate from *cis* to *trans* is relatively high. This is verified for high (4,000 K), room (298.15 K) and also for low temperatures (100 K). The most pronounced decrease in the rate corresponds to the HP-Ne complex, in which the decrease of the *trans*-barrier of just 0.0389 kcal/mol (see **Figure 6**) corresponds to a decrease



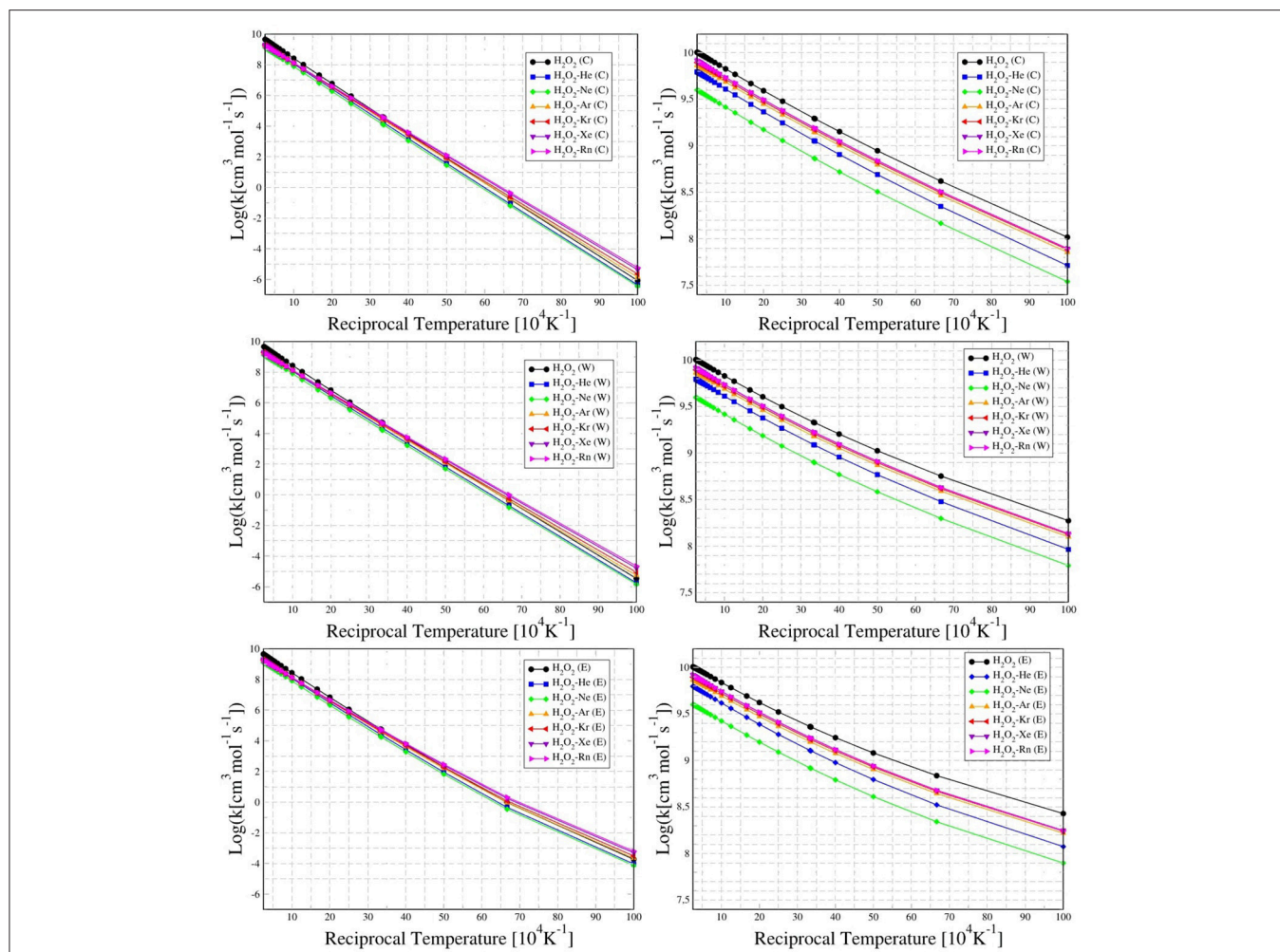


**FIGURE 6** | Temperature dependence (from 100 K up to 4,000 K) of the rate constant for conventional (C), Wigner (W), and Eckart (E) tunneling corrections, for *cis* to *trans* (left column) and *trans* to *cis* (right column) chiral conformations of H<sub>2</sub>O<sub>2</sub> and H<sub>2</sub>O<sub>2</sub>-Ng complexes.

**TABLE 4** | Adjusted parameters for the modified Arrhenius equation for conventional (C), Wigner (W) and Eckart (E) models with  $E_a$  in kcal/mol.

| Molecule             | A(C)                 | A(W)                 | A(E)                  | n(C)   | n(W)   | n(E)   | $E_a$ (C) | $E_a$ (W) | $E_a$ (E) |
|----------------------|----------------------|----------------------|-----------------------|--------|--------|--------|-----------|-----------|-----------|
| <b>CIS-BARRIER</b>   |                      |                      |                       |        |        |        |           |           |           |
| HP                   | $6.1018 \times 10^9$ | $2.8802 \times 10^9$ | $11.0401 \times 10^7$ | 0.0780 | 0.1650 | 0.5572 | 7.3552    | 7.0124    | 6.1979    |
| HP-He                | $2.6279 \times 10^9$ | $1.2418 \times 10^9$ | $4.8886 \times 10^7$  | 0.0759 | 0.1627 | 0.5517 | 7.3155    | 6.9737    | 6.1659    |
| HP-Ne                | $1.7572 \times 10^9$ | $0.8310 \times 10^9$ | $3.3715 \times 10^7$  | 0.0755 | 0.1622 | 0.5476 | 7.2742    | 6.9333    | 6.1322    |
| HP-Ar                | $2.6503 \times 10^9$ | $1.2611 \times 10^9$ | $6.2821 \times 10^7$  | 0.0732 | 0.1593 | 0.5200 | 7.0818    | 6.7464    | 5.9960    |
| HP-Kr                | $2.5508 \times 10^9$ | $1.2177 \times 10^9$ | $6.7090 \times 10^7$  | 0.0726 | 0.1584 | 0.5070 | 6.9795    | 6.6470    | 5.9211    |
| HP-Xe                | $2.4190 \times 10^9$ | $1.1593 \times 10^9$ | $7.2082 \times 10^7$  | 0.0721 | 0.1574 | 0.4915 | 6.8421    | 6.5129    | 5.8164    |
| HP-Rn                | $2.3730 \times 10^9$ | $1.1396 \times 10^9$ | $7.5261 \times 10^7$  | 0.0720 | 0.1571 | 0.4839 | 6.7739    | 6.4465    | 5.7646    |
| <b>TRANS-BARRIER</b> |                      |                      |                       |        |        |        |           |           |           |
| HP                   | $6.1504 \times 10^9$ | $4.1827 \times 10^9$ | $3.6443 \times 10^9$  | 0.0758 | 0.1212 | 0.1376 | 0.9082    | 0.7686    | 0.6923    |
| HP-He                | $3.7940 \times 10^9$ | $2.5942 \times 10^9$ | $2.3349 \times 10^9$  | 0.0764 | 0.1212 | 0.1340 | 0.9519    | 0.8145    | 0.7657    |
| HP-Ne                | $2.4228 \times 10^9$ | $1.6587 \times 10^9$ | $1.5061 \times 10^9$  | 0.0760 | 0.1207 | 0.1324 | 0.9413    | 0.8044    | 0.7575    |
| HP-Ar                | $4.4132 \times 10^9$ | $3.0523 \times 10^9$ | $2.7009 \times 10^9$  | 0.0775 | 0.1210 | 0.1357 | 0.9178    | 0.7851    | 0.7296    |
| HP-Kr                | $4.6795 \times 10^9$ | $3.2492 \times 10^9$ | $2.8867 \times 10^9$  | 0.0784 | 0.1214 | 0.1356 | 0.9177    | 0.7866    | 0.7325    |
| HP-Xe                | $4.8857 \times 10^9$ | $3.4004 \times 10^9$ | $3.0393 \times 10^9$  | 0.0791 | 0.1218 | 0.1354 | 0.9217    | 0.7915    | 0.7398    |
| HP-Rn                | $4.9038 \times 10^9$ | $3.4166 \times 10^9$ | $3.0635 \times 10^9$  | 0.0793 | 0.1218 | 0.1350 | 0.9227    | 0.7930    | 0.7424    |

**TABLE 5** | Adjusted parameters for the d-Arrhenius equation for conventional (C), Wigner (W) and Eckart (E) models with  $E_a$  in kcal/mol.

| Molecule             | A(C)               | A(W)               | A(E)               | d(C)    | d(W)    | d(E)    | $E_a$ (C) | $E_a$ (W) | $E_a$ (E) |
|----------------------|--------------------|--------------------|--------------------|---------|---------|---------|-----------|-----------|-----------|
| <b>CIS-BARRIER</b>   |                    |                    |                    |         |         |         |           |           |           |
| HP                   | $11.7 \times 10^9$ | $11.3 \times 10^9$ | $11.3 \times 10^9$ | -0.0013 | -0.0025 | -0.0143 | 7.5627    | 7.4084    | 8.0939    |
| HP-He                | $5.0 \times 10^9$  | $4.8 \times 10^9$  | $5.7 \times 10^9$  | -0.0013 | -0.0025 | -0.0143 | 7.5174    | 7.3641    | 8.0431    |
| HP-Ne                | $3.3 \times 10^9$  | $3.2 \times 10^9$  | $3.8 \times 10^9$  | -0.0013 | -0.0025 | -0.0143 | 7.4753    | 7.3227    | 7.9943    |
| HP-Ar                | $4.9 \times 10^9$  | $4.7 \times 10^9$  | $5.5 \times 10^9$  | -0.0013 | -0.0026 | -0.0142 | 7.2768    | 7.1297    | 7.7525    |
| HP-Kr                | $4.7 \times 10^9$  | $4.5 \times 10^9$  | $5.3 \times 10^9$  | -0.0013 | -0.0026 | -0.0142 | 7.1726    | 7.6274    | 7.6274    |
| HP-Xe                | $4.4 \times 10^9$  | $4.3 \times 10^9$  | $4.9 \times 10^9$  | -0.0014 | -0.0027 | -0.0142 | 6.8421    | 6.5129    | 7.4631    |
| HP-Rn                | $4.3 \times 10^9$  | $4.2 \times 10^9$  | $4.8 \times 10^9$  | -0.0014 | -0.0028 | -0.0143 | 6.9644    | 6.8252    | 7.3822    |
| <b>TRANS-BARRIER</b> |                    |                    |                    |         |         |         |           |           |           |
| HP                   | $11.7 \times 10^9$ | $11.3 \times 10^9$ | $11.8 \times 10^9$ | -0.0731 | -0.1578 | -0.2131 | 1.1387    | 1.1583    | 1.1603    |
| HP-He                | $7.3 \times 10^9$  | $7.3 \times 10^9$  | $7.4 \times 10^9$  | -0.0731 | -0.1414 | -0.1796 | 1.1822    | 1.1992    | 1.2210    |
| HP-Ne                | $4.6 \times 10^9$  | $4.6 \times 10^9$  | $4.7 \times 10^9$  | -0.0743 | -0.1441 | -0.1816 | 1.1705    | 1.1879    | 1.2079    |
| HP-Ar                | $8.5 \times 10^9$  | $8.6 \times 10^9$  | $8.6 \times 10^9$  | -0.0791 | -0.1510 | -0.1959 | 1.1520    | 1.1715    | 1.1928    |
| HP-Kr                | $9.1 \times 10^9$  | $9.1 \times 10^9$  | $9.2 \times 10^9$  | -0.0798 | -0.0026 | -0.1944 | 1.1545    | 1.1743    | 1.1950    |
| HP-Xe                | $9.6 \times 10^9$  | $9.6 \times 10^9$  | $9.7 \times 10^9$  | -0.0797 | -0.1497 | -0.1909 | 1.1605    | 1.1805    | 1.2007    |
| HP-Rn                | $9.6 \times 10^9$  | $9.6 \times 10^9$  | $9.7 \times 10^9$  | -0.0796 | -0.1491 | -0.1894 | 1.1619    | 1.1818    | 1.2017    |

**TABLE 6** | Difference between heights of *trans*-barrier of HP and HP-Ng complexes and relative decrease of the transition rate of *cis* to *trans* configuration for representative temperatures (4,000, 298.15, and 100 K).

| Molecule | $\Delta$ (kcal/mol) (a) | Decrease of rate (%) |                   |                |
|----------|-------------------------|----------------------|-------------------|----------------|
|          |                         | ( $T = 4,000$ K)     | ( $T = 298.15$ K) | ( $T = 100$ K) |
| HP       | 0                       | 0                    | 0                 | 0              |
| HP-He    | 0.0501                  | 50.39                | 42.48             | 38.32          |
| HP-Ne    | 0.0389                  | 66.66                | 62.66             | 60.67          |
| HP-Ar    | 0.0224                  | 31.07                | 28.68             | 27.26          |
| HP-Kr    | 0.0250                  | 26.50                | 24.02             | 22.34          |
| HP-Xe    | 0.0310                  | 24.45                | 20.90             | 18.47          |
| HP-Rn    | 0.0322                  | 24.53                | 20.70             | 18.10          |

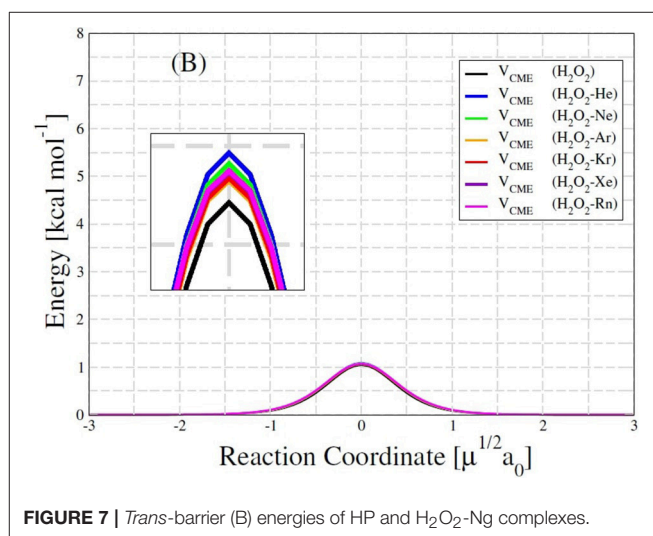
$$^{(a)} \Delta = E_{b-trans}(HP) - E_{b-trans}(HP-Ng).$$

of over 60% for the *cis-trans* transition rate, followed by HP-He. It is also interesting to note that this small change in energy barrier but with a substantial change in rate was also observed for other HP-Ng complexes. For example, HP-Ar complex showed a decrease of just 0.0224 kcal/mol but a 28.68% decrease of rate at 100 K.

Finally, at a temperature close to 300K, the Boltzmann distribution shows that about 16% of HP's population has higher energy than the *trans*-barrier with thermal fluctuations of approximately 1.7686 kcal/mol (Ball and Brindley, 2016). It has also been found that at low temperatures the chiral interconversion quantum encapsulation time of HP is very small. At a temperature of 100 K this time is <1 pico-second (Bitencourt et al., 2008), and at temperatures close to 0 K which can reach 3 pico-seconds.

## 4. CONCLUSIONS

The obtained results indicate that the chiral transition rate of *trans* to *cis* configuration of hydrogen peroxide

**FIGURE 7** | *Trans*-barrier (B) energies of HP and H<sub>2</sub>O<sub>2</sub>-Ng complexes.

in the presence of the noble gases He and Ne were the lowest over the entire temperature range of 4,000–100 K.

The AIM analysis shows that the interaction between H<sub>2</sub>O<sub>2</sub> and the noble gases should be a van der Waals type. Although the H<sub>2</sub>O<sub>2</sub> acts as an acid in the context of this investigation, the high hardness and high electronegativity of the noble gases hold their electrons very tight to permit a covalence bond between H<sub>2</sub>O<sub>2</sub> and Ng. On the other hand, it seems that both He and Ne are better able to affect the hyperconjugation effect and destabilizing repulsion among the lone pairs that are responsible for rotational barriers (Song et al., 2005). This may explain why the chiral transition rate decreases more for the complexes composed by Ne and He atoms, the hardest and more electronegative noble gases (Furtado et al., 2015).

Finally, the *trans*-barrier plays an important role because it is much smaller than the *cis*-barrier. The results showed that a small increase in the *trans*-barrier height in the complexes is responsible for a significant decrease in the rate of transition from *cis* to *trans*. Thus, these effects may contribute to the feasibility of separating one or the other enantiomer of the H<sub>2</sub>O<sub>2</sub> molecule.

## AUTHOR CONTRIBUTIONS

RG conceived and supervised the study. RG also helped write the paper. YS performed the H<sub>2</sub>O<sub>2</sub>-Ng electronic and thermal chiral rate calculations. PN determined the H<sub>2</sub>O<sub>2</sub>-Ng minimum and transition state configurations and LdM used the AIM theory

## REFERENCES

- Allen, L. C. (1989). Electronegativity is the average one-electron energy of the valence-shell electrons in ground-state free atoms. *J. Am. Chem. Soc.* 111, 9003–9014. doi: 10.1021/ja00207a003
- Allen, L. C., and Huheey, J. E. (1980). The definition of electronegativity and the chemistry of the noble gases. *J. Inorg. Nuclear Chem.* 42, 1523–1524. doi: 10.1016/0022-1902(80)80132-1
- Al-Refaie, A. F., Ovsyannikov, R. I., Polyansky, O. L., Yurchenko, S. N., and Tennyson, J. (2015). A variationally calculated room temperature line-list for H<sub>2</sub>O<sub>2</sub>. *J. Mol. Spectrosc.* 318, 84–90. doi: 10.1016/j.jms.2015.10.004
- Antunes, F., and Brito, P. M. (2017). Quantitative biology of hydrogen peroxide signaling. *Redox Biol.* 13, 1–7. doi: 10.1016/j.redox.2017.04.039
- Aquilanti, V., Bartolomei, M., Pirani, F., Cappelletti, D., Vecchiocattivi, F., Shimizu, Y., et al. (2005). Orienting and aligning molecules for stereochemistry and photodynamics. *Phys. Chem. Chem. Phys.* 7, 291–300. doi: 10.1039/B415212C
- Aquilanti, V., Mundim, K. C., Elango, M., Kleijn, S., and Kasai, T. (2010). Temperature dependence of chemical and biophysical rate processes: Phenomenological approach to deviations from arrhenius law. *Chem. Phys. Lett.* 498, 209–213. doi: 10.1016/j.cplett.2010.08.035
- Atkins, P., De Paula, J., and Friedman, R. (2013). *Physical Chemistry: Quanta, Matter, and Change*. New York, NY: Oxford University Press.
- Bader, R. F. (1991). A quantum theory of molecular structure and its applications. *Chem. Rev.* 91, 893–928. doi: 10.1021/cr00005a013
- Ball, R., and Brindley, J. (2016). The life story of hydrogen peroxide iii: chirality and physical effects at the dawn of life. *Orig. Life Evol. Biospheres* 46, 81–93. doi: 10.1007/s11084-015-9465-y
- Barreto, P. R., Palazzetti, F., Grossi, G., Lombardi, A., Maciel, G., and Vilela, A. (2010). Range and strength of intermolecular forces for van der waals complexes of the type h<sub>2</sub>xn-rg, with x = o, s and n = 1, 2. *Int. J. Quantum Chem.* 110, 777–786. doi: 10.1002/qua.22127
- Barreto, P. R., Vilela, A. F., Lombardi, A., Maciel, G. S., Palazzetti, F., and Aquilanti, V. (2007). The hydrogen peroxide- rare gas systems: Quantum chemical calculations and hyperspherical harmonic representation of the potential energy surface for atom- floppy molecule interactions. *J. Phys. Chem. A* 111, 12754–12762. doi: 10.1021/jp076268v
- Bell, R. (1980). *The Tunnel Effect in Chemistry*.
- Bell, R. P. (1959). The tunnel effect correction for parabolic potential barriers. *Trans. Faraday Soc.* 55, 1–4. doi: 10.1039/tf9595500001
- Bitencourt, A. C., Ragni, M., Maciel, G. S., Aquilanti, V., and Prudente, F. V. (2008). Level distributions, partition functions, and rates of chirality changing processes for the torsional mode around o–o bonds. *J. Chem. Phys.* 129:154316. doi: 10.1063/1.2992554
- Boys, S. F., and Bernardi, F. d. (1970). The calculation of small molecular interactions by the differences of separate total energies. some procedures with reduced errors. *Mol. Phys.* 19, 553–566. doi: 10.1080/00268977000101561
- Carlson, R., Anderson, M., Johnson, R., Smythe, W., Hendrix, A., Barth, C., et al. (1999). Hydrogen peroxide on the surface of europa. *Science* 283, 2062–2064. doi: 10.1126/science.283.5410.2062
- to perform the H<sub>2</sub>O<sub>2</sub>-Ng topological analyses and wrote the manuscript, which was reviewed by all authors.

## ACKNOWLEDGMENTS

We gratefully acknowledge the financial support from the Brazilian Research Councils CNPq and FAPDF.

## SUPPLEMENTARY MATERIAL

The Supplementary Material for this article can be found online at: <https://www.frontiersin.org/articles/10.3389/fchem.2018.00671/full#supplementary-material>

- Carvalho-Silva, V. H., Aquilanti, V., de Oliveira, H. C., and Mundim, K. C. (2017). Deformed transition-state theory: Deviation from a rrhenius behavior and application to bimolecular hydrogen transfer reaction rates in the tunneling regime. *J. Comput. Chem.* 38, 178–188. doi: 10.1002/jcc.24529
- Cortés-Guzmán, F., and Bader, R. F. (2005). Complementarity of qtaim and mo theory in the study of bonding in donor–acceptor complexes. *Coord. Chem. Rev.* 249, 633–662. doi: 10.1016/j.ccr.2004.08.022
- Daza, M. C., Dobado, J., Molina, J. M., and Villaveces, J. L. (2000). Structure and bonding of h<sub>2</sub> o 2... x complexes with (x = no+, cn-, hcn, hnc, co). *Phys. Chem. Chem. Phys.* 2, 4089–4094. doi: 10.1039/b001885f
- Dobado, J., Martínez-García, H., Molina, J. M., and Sundberg, M. R. (1998). Chemical bonding in hypervalent molecules revised. application of the atoms in molecules theory to y<sub>3</sub> x and y<sub>3</sub> xz (y = h or ch<sub>3</sub>; x = n, p or as; z = o or s) compounds. *J. Am. Chem. Soc.* 120, 8461–8471. doi: 10.1021/ja980141p
- Dobado, J., and Molina, J. (1999). Adenine- hydrogen peroxide system: Dft and mp2 investigation. *J. Phys. Chem. A* 103, 4755–4761. doi: 10.1021/jp990671n
- Dobado, J., and Molina, J. M. (1993). Ab initio molecular orbital calculation of the hydrogen peroxide dimer: study of basis set superposition error. *J. Phys. Chem.* 97, 7499–7504. doi: 10.1021/j100131a018
- Dunning, T. H. Jr. (1989). Gaussian basis sets for use in correlated molecular calculations. i. the atoms boron through neon and hydrogen. *J. Chem. Phys.* 90, 1007–1023. doi: 10.1063/1.456153
- Eckart, C. (1930). The penetration of a potential barrier by electrons. *Phys. Rev.* 35:1303.
- Encrenaz, T., Bézard, B., Greathouse, T., Richter, M., Lacy, J., Atreya, S., et al. (2004). Hydrogen peroxide on mars: evidence for spatial and seasonal variations. *Icarus* 170, 424–429. doi: 10.1016/j.icarus.2004.05.008
- Eyring, H. (1935). The activated complex in chemical reactions. *J. Chem. Phys.* 3, 107–115. doi: 10.1063/1.1749604
- Fehrens, B., Luckhaus, D., and Quack, M. (2007). Stereomutation dynamics in hydrogen peroxide. *Chem. Physics*, 338, 90–105. doi: 10.1016/j.chemphys.2007.06.012
- Frisch, M. J., Trucks, G. W., Schlegel, H. B., Scuseria, G. E., Robb, M. A., Cheeseman, J. R., et al. (2009) *Gaussian 09 Revision e.01*. Wallingford, CT: Gaussian Inc.
- Furtado, J., De Proft, F., and Geerlings, P. (2015). The noble gases: how their electronegativity and hardness determines their chemistry. *J. Phys. Chem.* 119, 1339–1346. doi: 10.1021/jp5098876
- Goebel, J., Ault, B. S., and Del Bene, J. E. (2000). Matrix isolation and *ab initio* study of the hydrogen-bonded complex between h<sub>2</sub>o<sub>2</sub> and (ch<sub>3</sub>)<sub>2</sub> o. *J. Phys. Chem.* 104, 2033–2037. doi: 10.1021/jp9941716
- Goebel, J. R., Antle, K. A., Ault, B. S., and Del Bene, J. E. (2002). Matrix isolation and *ab initio* study of 1: 1 hydrogen-bonded complexes of h<sub>2</sub>o<sub>2</sub> with hf, hcl, and hbr. *J. Phys. Chem.* 106, 6406–6414. doi: 10.1021/jp020520b
- Goebel, J. R., Ault, B. S., and Del Bene, J. E. (2001a). Matrix isolation and *ab initio* study of 1: 1 hydrogen-bonded complexes of h<sub>2</sub>o<sub>2</sub> with nh<sub>3</sub> and n (ch<sub>3</sub>)<sub>3</sub>. *J. Phys. Chem.* 105, 6430–6435. doi: 10.1021/jp010813p
- Goebel, J. R., Ault, B. S., and Del Bene, J. E. (2001b). Matrix isolation and *ab initio* study of 1: 1 hydrogen-bonded complexes of h<sub>2</sub>o<sub>2</sub> with phosphorus and sulfur bases. *J. Phys. Chem.* 105, 11365–11370. doi: 10.1021/jp013262

- González, L., Mó, O., and Yáñez, M. (1997). High-level *ab initio* versus dft calculations on (h<sub>2</sub>o<sub>2</sub>)<sub>2</sub> and h<sub>2</sub>o<sub>2</sub>-h<sub>2</sub>o complexes as prototypes of multiple hydrogen bond systems. *J. Comput. Chem.* 18, 1124–1135.
- Grzechnik, K., Mierzwicki, K., and Mielke, Z. (2013). Matrix-isolated hydrogen-bonded and van der waals complexes of hydrogen peroxide with ocs and cs<sub>2</sub>. *ChemPhysChem* 14, 777–787. doi: 10.1002/cphc.201200696
- Henkelman, G., Jóhannesson, G., and Jónsson, H. (2002). “Methods for finding saddle points and minimum energy paths,” in *Theoretical Methods in Condensed Phase Chemistry*, ed S. D. Schwartz (Dordrecht: Springer), 269–302.
- Hunt, R. H., Leacock, R. A., Peters, C. W., and Hecht, K. T. (1965). Internal-rotation in hydrogen peroxide: the far-infrared spectrum and the determination of the hindering potential. *J. Chem. Phys.* 42, 1931–1946. doi: 10.1063/1.1696228
- Keith, T. A. (2017). *Aimall (version 17.11.04)*. TK gristmill software: Overland Park, KS. Available online at: aim.tkgristmill.com
- Leal, L. A., da Cunha, W. F., Roncaratti, L. F., Silva, G. M. E., and Gargano, R. (2016). H<sub>2</sub>O<sub>2</sub>-ng dynamics predictions using an accurate potential energy surface. *Mol. Phys.* 114, 440–445. doi: 10.1080/00268976.2015.1078507
- Lewis, W. M. (1967). “Studies in catalysis. Part ix. the calculation in absolute measure of velocity constants and equilibrium constants in gaseous systems,” in *Selected Readings in Chemical Kinetics*, eds M. H. Back and K. J. Laidler (Pergamon: Elsevier), 36–40.
- Lombardi, A. and Palazzetti, F. (2018). Chirality in molecular collision dynamics. *J. Phys. Condensed Matter* 30:063003. doi: 10.1088/1361-648X/aaa1c8
- Lombardi, A., Palazzetti, F., Maciel, G., Aquilanti, V., and Sevryuk, M. (2011). Simulation of oriented collision dynamics of simple chiral molecules. *Int. J. Quantum Chem.* 111, 1651–1658. doi: 10.1002/qua.22816
- Lundell, J., Jolkkonen, S., Khriachtchev, L., Pettersson, M., and Räsänen, M. (2001). Matrix isolation and *ab initio* study of the hydrogen-bonded h<sub>2</sub>o<sub>2</sub>-co complex. *Chem. Eur. J.* 7, 1670–1678. doi: 10.1002/1521-3765(20010417)7:8<1670::AID-CHEM16700>3.0.CO;2-N
- Lundell, J., Pehkonen, S., Pettersson, M., and Räsänen, M. (1998). Interaction between hydrogen peroxide and molecular nitrogen. *Chem. Phys. Lett.* 286, 382–388. doi: 10.1016/S0009-2614(98)00003-7
- Maciel, G. S., Bitencourt, A. C. P., Ragni, M., and Aquilanti, V. (2006). Studies of the dynamics around the o–o bond: orthogonal local modes of hydrogen peroxide. *Chem. Phys. Lett.* 432, 383–390. doi: 10.1016/j.cplett.2006.10.073
- Malyszek, P., and Koput, J. (2013). Accurate *ab initio* potential energy surface and vibration-rotation energy levels of hydrogen peroxide. *J. Comput. Chem.* 34, 337–345. doi: 10.1002/jcc.23137
- Matta, C. and Boyd, R. (2007). *Quantum Theory of Atoms in Molecules: Recent Progress in Theory and Application*. New York, NY: Wiley-VCH.
- Mo, O., Yanez, M., Rozas, I., and Elguero, J. (1994). Structure, vibrational frequencies, and thermodynamic properties of hydrogen peroxide dimers: an *ab initio* molecular orbital study. *J. Chem. Phys.* 100, 2871–2877. doi: 10.1063/1.466429
- Molina, J. M., Dobado, J. A., Daza, M. C., and Villaveces, J. L. (2002). Structure and bonding of weak hydrogen peroxide complexes. *J. Mol. Struct.* 580, 117–126. doi: 10.1016/S0166-1280(01)00602-9
- Mucha, M., and Mielke, Z. (2009). Photochemistry of the glyoxal-hydrogen peroxide complexes in solid argon: formation of 2-hydroxy-2-hydroperoxyethanal. *Chem. Phys. Lett.* 482, 87–92. doi: 10.1016/j.cplett.2009.09.082
- Palazzetti, F., Tsai, P.-Y., Lombardi, A., Nakamura, M., Che, D.-C., Kasai, T., et al. (2013). Aligned molecules: chirality discrimination in photodissociation and in molecular dynamics. *Rendiconti Lincei* 24, 299–308. doi: 10.1007/s12210-013-0248-y
- Pehkonen, S., Lundell, J., Khriachtchev, L., Pettersson, M., and Räsänen, M. (2004). Matrix isolation and quantum chemical studies on the h<sub>2</sub>o<sub>2</sub>-so<sub>2</sub> complex. *Phys. Chem. Chem. Phys.* 6, 4607–4613. doi: 10.1039/B410223A
- Peterson, K. A., Figgen, D., Goll, E., Stoll, H., and Dolg, M. (2003). Systematically convergent basis sets with relativistic pseudopotentials. ii. small-core pseudopotentials and correlation consistent basis sets for the post-d group 16–18 elements. *J. Chem. Phys.* 119, 11113–11123. doi: 10.1063/1.1622924
- Piatnytskyi, D., Zdorevsky, O., Perepelytsya, S., and Volkov, S. (2016). Formation of complexes of hydrogen peroxide molecules with dna. *Ukr. J. Phys.* 61, 219–225. doi: 10.15407/ujpe61.03.0219
- Polanyi, M. and Wigner, E. (1928). Über die interferenz von eigenschwingungen als ursache von energieschwankungen und chemischer umsetzungen. *Zeitschrift für Phys. Chem.* 139, 439–452. doi: 10.1515/zpch-1928-13930
- Ramalho, S. S., da Cunha, W. F., Barreto, P. R., Neto, P. H., Roncaratti, L. F., e Silva, G. M., and Gargano, R. (2011). Thermal rate constant calculation of the nf+ f reactive system multiple arrangements. *J. Phys. Chem.* 115, 8248–8254. doi: 10.1021/jp204229d
- Roncaratti, L., Leal, L., Pirani, F., Aquilanti, V., e Silva, G., and Gargano, R. (2014). Chirality of weakly bound complexes: the potential energy surfaces for the hydrogen-peroxide- noble-gas interactions. *J. Chem. Phys.* 141:134309. doi: 10.1063/1.4897136
- Roncaratti, L. F. and Aquilanti, V. (2010). Whittaker–hill equation, ince polynomials, and molecular torsional modes. *Int. J. Quantum Chem.* 110, 716–730. doi: 10.1002/qua.22255
- Roohi, H., Nowroozi, A., Bavafa, S., Akbary, F., and Eshghi, F. (2010). Interaction between nh<sub>2</sub>no and h<sub>2</sub>o<sub>2</sub>: a quantum chemistry study. *Int. J. Quantum Chem.* 110, 1972–1981. doi: 10.1002/qua.22364
- Shi, Y. and Zhou, Z.-Y. (2004). Density functional theory study of the hydrogen bonding interaction complexes of hydrogen peroxide with glycine. *J. Mol. Struct.* 674, 113–119. doi: 10.1016/j.theochem.2003.12.018
- Sies, H. (2017). Hydrogen peroxide as a central redox signaling molecule in physiological oxidative stress: oxidative eustress. *Redox Biol.* 11, 613–619. doi: 10.1016/j.redox.2016.12.035
- Silva, V. H., Aquilanti, V., de Oliveira, H. C., and Mundim, K. C. (2013). Uniform description of non-arrhenius temperature dependence of reaction rates, and a heuristic criterion for quantum tunneling vs classical non-extensive distribution. *Chem. Phys. Lett.* 590, 201–207. doi: 10.1016/j.cplett.2013.10.051
- Song, L., Liu, M., Wu, W., Zhang, Q., and Mo, Y. (2005). Origins of rotational barriers in hydrogen peroxide and hydrazine. *J. Chem. Theory Comput.* 1, 394–402. doi: 10.1021/ct049843x
- Su, T.-M., Palazzetti, F., Lombardi, A., Grossi, G., and Aquilanti, V. (2013). Molecular alignment and chirality in gaseous streams and vortices. *Rendiconti Lincei* 24, 291–297. doi: 10.1007/s12210-013-0249-x
- Truhlar, D. G., Garrett, B. C., and Klippenstein, S. J. (1996). Current status of transition-state theory. *J. Phys. Chem.* 100, 12771–12800. doi: 10.1021/jp953748q
- Truhlar, D. G., Isaacson, A. D., and Garrett, B. C. (1985). *Generalized Transition State Theory, Volume 4*. Boca Raton, FL: CRC Press.
- Wang, C., Zhang, D. H., and Skodje, R. T. (2012). A six-dimensional wave packet study of the vibrational overtone induced decomposition of hydrogen peroxide. *J. Chem. Phys.* 136:164314. doi: 10.1063/1.4705755
- Wilson, A. K., Woon, D. E., Peterson, K. A., and Dunning, T. H. Jr. (1999). Gaussian basis sets for use in correlated molecular calculations. ix. The atoms gallium through krypton. *J. Chem. Phys.* 110, 7667–7676. doi: 10.1063/1.478678
- Woon, D. E., and Dunning Jr, T. H. (1993). Gaussian basis sets for use in correlated molecular calculations. iii. The atoms aluminum through argon. *J. Chem. Phys.* 98, 1358–1371. doi: 10.1063/1.464303
- Yu, C.-Y., and Yang, Z.-Z. (2011). A systemic investigation of hydrogen peroxide clusters (h<sub>2</sub>o<sub>2</sub>)<sub>n</sub> (n= 1- 6) and liquid-state hydrogen peroxide: based on atom-bond electronegativity equalization method fused into molecular mechanics and molecular dynamics. *J. Phys. Chem.* 115, 2615–2626. doi: 10.1021/jp111284t

**Conflict of Interest Statement:** The authors declare that the research was conducted in the absence of any commercial or financial relationships that could be construed as a potential conflict of interest.

Copyright © 2019 Só, Neto, de Macedo and Gargano. This is an open-access article distributed under the terms of the Creative Commons Attribution License (CC BY). The use, distribution or reproduction in other forums is permitted, provided the original author(s) and the copyright owner(s) are credited and that the original publication in this journal is cited, in accordance with accepted academic practice. No use, distribution or reproduction is permitted which does not comply with these terms.